Asymmetric magnetization reversal and its dual origin in Co/FeMn out-of-plane induced exchanged bias systems

Yang Liu, Shou-Guo Wang, Yang Li, Ning Li, Shuai Liu, Ning Chen, Ming-Hua Li, and Guang-Hua Yu

Phys. Rev. B **84**, 104436 — Published 21 September 2011

DOI: 10.1103/PhysRevB.84.104436

Novel Asymmetric Magnetization Reversal and Its Dual Origin in out-of-plane induced Co/FeMn Exchange Bias Systems

Yang Liu[1], Shou-Guo Wang[2], Yang Li[3], Ning Li[1], Shuai Liu[1], Ning Chen[1], Ming-Hua Li[1], Guang-Hua Yu[1,*]

[1]*Department of Materials Physics and Chemistry, University of Science and Technology Beijing, Beijing 100083, China*

[2]*State Key Laboratory of Magnetism, Beijing National Laboratory for Condensed Matter Physics, Institute of Physics, Chinese Academy of Sciences, Beijing 100190, China*

[3]*Department of Engineering Science and Materials, University of Puerto Rico at Mayaguez, Mayagues, PR 00681-9044, USA*

The comprehension on the origins of the asymmetric behavior during the magnetization reversal is an outstanding issue in the studies of exchange bias (EB). By far, two intrinsic origins of the asymmetric magnetization reversal behavior (AMRB) have been found in different systems separately. The compatibility of the two origins has not been proved, yet. Here we report the AMRBs derived from the cooperation between both of the two AMRB origins. Novel AMRBs, including the odd shape of the hysteresis loops and a positive EB, were found in the Co/FeMn bilayers grown under a perpendicular magnetic field. The striking AMRBs we observed could be explained by a model based on spin incoherent rotation and antiferromagnetic interfacial coupling. It suggests that both of the two AMRB origins are indispensable in the development of these unique AMRBs.

Exchange bias (EB) means that the hysteresis loop of the ferromagnetic/antiferromagnetic (FM/AFM) nanostructures shifts along the magnetic field axis below the blocking temperature (T_B). Because of the pinning of the interfacial uncompensated AFM spins (UCAS) below T_B, a unidirectional anisotropy is induced to the FM layer through the FM/AFM interfacial coupling, which changes the symmetry of the FM magnetic anisotropy. Besides the asymmetry of the hysteresis loop, a variety of asymmetric characters have been observed during the magnetization reversal in diverse EB systems [1-6].

The asymmetric magnetization reversal behavior (AMRB) is a significant nature of the EB systems. It has been revealed that the forward and backward branches of the magnetization reversal are performed in different modes, such as the separated ways of magnetic moment rotation [5-8], the distinct nucleation sites and abilities of the inverse domain [9-18], and the unsymmetrical training and recovering effect of the pinning of the UCAS [3,19-22]. Most AMRBs, except for the loop shift, have their particular features in the specific EB systems, which strongly depends on the structure [1,4,23,24] and measuring methods [4,9-11,25-28]. The appearances of the AMRBs are so complex that the comprehension on the origin and the classification of the AMRBs is still in debate.

Theoretical studies [4-6] have already shown two intrinsic origins of AMRB, which are responsible for two types of AMRBs, respectively. The origin for type-I AMRBs is the inhomogeneity of the ferromagnetic structure [1,4], while the origin for type-II AMRBs is the competition of the uniaxial FM anisotropy (K_U), the interfacial unidirectional exchange anisotropy (K_E), and the magnetic field (H) [5,6]. Accordingly, type-I AMRBs are often observed as asymmetric incoherent reversal when the FM layer has adequate thickness (t_{FM}) and insufficient exchange stiffness (A_{ex}). The incoherence of the FM layer during the reversal process has been intensively studied by experiment and micromagnetic simulation [4]. Meanwhile, type-II AMRBs is observed as asymmetric coherent rotation. In most previous studies, the pinning direction (PD) is along the FM easy-axis (K_U and K_E are collinear). Then the AMRBs vary with the rotation of H, which can be well described by a shifted Stoner-Wohlfarth (S-W) asteroid [6].

However, the two AMRB origins used to be found individually in different EB systems. Each AMRB origin leads to a particular kind of AMRBs. Neither of them could explain all the AMRBs. So far, a universal understanding on the intricate AMRBs is still lacking. In this letter, the uniformity and compatibility of the two AMRB origins are investigated. Novel AMRBs, including a positive exchange bias, were observed in the Co/FeMn bilayer with a thick Co layer and oblique exchange anisotropy. It indicates that the two AMRB origins could coexist and cooperate in our Co/FeMn bilayers. Both of them are indispensable for the development of the novel AMRBs.

The Co(t_{Co})/FeMn(25.0 nm) and Co(8.0 nm)/FeMn(t_{FeMn}) bilayer samples were magnetron sputtered under an inducing magnetic field (about −800 Oe) perpendicular to the film plane. The inducing field is much less than the value of perpendicular saturation field. Therefore, the alignment of the Co interfacial moments are tilted when the EB is established, resulting in an

oblique PD. So the conditions for both AMRB origins (One is the angular competition of K_U, K_E, and H, while the other is the incoherent reversal of the FM layer) are fulfilled. The hysteresis loops were measured by a MicroMag2900 Alternating Gradient Force Magnetometer (AGM) along the perpendicular direction. Owing to the cooperation of the two AMRB origins, the loops exhibit unique asymmetric characters. However, these unique AMRBs were not observed in the results measured by the Vibrating Sample Magnetometer (VSM) in the Quantum Design Physical Property Measurement System (PPMS).

Figure 1 shows the *M*-*H* curves of the Co(t_{Co})/FeMn(13.0 nm) multilayers, measured by VSM (in PPMS) along two in-plane directions perpendicular to each other. There is a remarkable excess of the nominal saturation magnetization (μ_s/V_{Co}) than the ideal bulk Co should have (about 1440 Gs), especially when the Co layer is ultrathin, which implies a large amount of uncompensated spins near the FM/AFM interface in FeMn layer. Figure 2 shows the *M*-*H* curves of the Co(t_{Co})/FeMn(13.0 nm) multilayers measured by VSM (in PPMS) along the direction perpendicular to the film plane. The perpendicular *M*-*H* curves for t_{Co}<6.4 nm show a rounded hard-axis loop, implying the incoherent rotation of the FM magnetic moments under the pinning effect of the AFM layer. Whereas the loop curves for t_{Co}>6.4 nm are of typical broken line representing the coherent hard-axis reversal. It can be seen that the thinner the Co layer is, the more rounded is the loop shape. The nominal saturation magnetizations along the perpendicular direction are also more than the normal value when the Co layer is thin. The dependences of the nominal saturation magnetizations on t_{Co} along the in-plane and perpendicular directions are shown in Fig.3. The inset of Fig.3 shows the perpendicular saturation magnetizations for t_{Co}<6.4 nm measured by AGM. The perpendicular saturation field for t_{Co}>6.4 nm beyond the maximum of the measuring field of the AGM we used (15 kOe). Both the AGM and the VSM (in PPMS) measurement indicate that the uncompensated spins in the FeMn layer originated from the FM/AFM interfacial coupling makes a considerable contribution on the saturation magnetization as much as that of 7~10 Co monolayers.

Surprisingly, hysteresis loops of the Co(t_{Co})/FeMn(25.0 nm) bilayers measured by AGM along the perpendicular direction exhibit novel AMRBs. As shown in Fig.4, two “Peaks” of magnetization (*M*) appears in loop (C) (t_{Co}=8.0 nm). This asymmetric feature is also observed when t_{Co}=6.4 nm and t_{Co}=10.0 nm (not shown in the Figure), and fades out after t_{Co}>10.0 nm. Loop (D) (t_{Co}=12.8 nm) is nearly a typical hard-axis loop of coherent rotation, except for a tiny, almost imperceptible, asymmetric feature near the center of the loop. It is notable that loop (B) (t_{Co}=3.2 nm) contains two small hysteresis regions in the first and the third quadrant symmetrically (marked by arrows in the figure), which is also a typical character of antiferromagnetic coupling. Since the loop shape is symmetric when t_{Co}<3.2 nm, this anomaly in loop (B) seems like a sign before the emergence of the AMRB with the increment of t_{Co}. It suggests that the odd AMRB in this system has a critical range of Co layer thickness, which should be associated with the inhomogeneity of the FM magnetic structures.

Moreover, there is also a particular AFM critical thickness (t_c^{AFM}) for this novel AMRB, which is independent of the conventional t_c^{AFM} for the loop shift. The evolution of the asymmetry characters in the perpendicular hysteresis loops for the Co(8.0 nm)/FeMn(t_{FeMn}) bilayers are shown in Fig.5. Similar to the common EB systems with collinear K_U and K_E, our Co/FeMn bilayer system with non-collinear K_U and K_E has a critical thickness of the AFM layer to exhibit the EB. The loops in Fig.5 are symmetric when t_{FeMn}<4.0 nm and are asymmetric when t_{FeMn}>6.0 nm, indicating that the t_c^{AFM} for the loop shift is between 4.0 and 6.0 nm. There is obvious hysteresis in the center of the loop when t_{FeMn}=6.0~9.0 nm. However, the odd *M*-peaks appears after t_{FeMn}>12.0 nm, which is much more than the conventional t_c^{AFM} for the loop shift.

Besides, a positive loop shift (shift along the inducing field direction) of the hysteresis zone is observed in loop (e) (t_{FeMn}=6.0 nm), which means positive exchange bias (PEB) exists when t_{FeMn} is slightly larger than the t_c^{AFM} for the loop shift. The PEB has already been found in several FM/AFM, FM/ferrimagnetic, soft/hard ferrimagnetic, and FM/spin-glass systems [29-33]. In some systems, such as FM/FeF_2 [29], the PEB appears at the whole low temperature region if only the inducing field is large enough. In some other systems, such as Co/CoO [30] and NiFe/IrMn [34], the PEB appears only at a critical region that the temperature is slightly lower than the blocking temperature and the AFM thickness is slightly larger than the critical AFM thickness at that temperature [35]. The domain distribution of the UCAS and the antiferromagnetic interfacial coupling (AFC) are responsible for the PEB in the above two cases respectively. Our results indicate that the Co/FeMn bilayers also could have PEB at the critical region. The PEB in our Co(8.0 nm)/FeMn(t_{FeMn}) bilayer appears at the AFM thickness region around t_{FeMn}=6.0 nm. Meanwhile, an indication of AFC is also found in loop (c) (t_{FeMn}=3.0 nm). The loop (c) has an inverse hysteresis zone in the center of *M*-*H* loop.

As the FeMn layer thickness increases, the loop (f) (t_{FeMn}=9.0 nm) exhibit a negative shift of the hysteresis zone. After t_{FeMn}>12.0 nm, unexpectedly, the asymmetry character is no longer just a horizontal loop shift. It can be seen in loop (g) and (h) that there are two *M*-peaks in each reversal branch respectively, which is attributed to the irreversible rotation of the magnetic moments.

However, the novel AMRBs mentioned above is only observed in the perpendicular measurement by means of AGM. The in-plane AGM measurement using small mangetic field were performed in order to examine the in-plane magnetization reversal behaviors. As shown in Fig.6 and Fig.7, the in-plane hysteresis loops exhibit obvious EB. The exchange bias field (H_{ex}) of the Co(t_{Co})/FeMn(13.0 nm) multilayers varies as expected. There is an intensity loss of the EB (H_{ex} is smaller than the H_{ex}~$1/t_{FM}$ law) when t_{Co}<1.6 nm. The H_{ex} reaches its maximum at t_{Co}=1.6 nm, then decays with the increment of t_{Co}. However, the signal of the loop shift is random, which means the PD could be any direction in the film plane. The loops of Co(8.0 nm)/FeMn(9.0 nm) and Co(8.0 nm)/FeMn(12.0 nm) have the two-step reversal character, which is often observed when the measuring direction (MD) is perpendicular to the PD, implying the existence of in-plane EB. There is barely EB when t_{FeMn}<6.0 nm and a small EB when t_{FeMn}=6.0 nm, indicating the

t_c^{AFM} for the in-plane loop shift is nearly 6.0 nm.

The in-plane VSM (in PPMS) measurement using small mangetic field were also performed. As shown in Fig.8 and Fig.9, taking account for the directional discrepancy of the measuring field, the features of the VSM results are similar to that of the AGM results. Although there are significant differences between the results measured by the AGM and the VSM along the perpendicular direction, the in-plane results measured by these two distinct apparatuses have almost the same characters. However, unlike the AGM in-plane results, the VSM in-plane loops of the Co(8 nm)/FeMn(t_{FeMn}) multilayers did not show two-step characters.

Further considering that the H_{ex} of the Co(8.0 nm)/FeMn(12.0 nm) multilayers in Fig.9 (nearly -60 Oe) is very close to the in-plane H_{ex} along the inducing field direction (about -64 Oe, measured by PPMS, not shown here), it can be known that the PD is out-of-plane, but close to the film plane. Therefore, the PDs in our samples are tilted and have random projection directions in the film plane. It means that the PD and the direction of the measuring field are non-collinear, which satisfy the condition for the type-II AMRB origin.

Meanwhile, the condition for the type-I AMRB origin (the inhomogeneity of the FM structure) is also satisfied. The incoherent reversal of the FM layer in different depth usually could be observed by detecting the spin configuration at the top and the bottom interfaces of the FM layer [4]. Analogously, in our Co/FeMn system, the inner magnetic structure of the Co layer also plays the key role in the magnetization reversal. It could be confirmed in the perpendicular induced $(Pt/Co)_n/Pt(t_{Pt})/Co/FeMn$ systems by tuning the interlayer coupling between the $(Pt/Co)_n$ periods and the thick Co single layer through the Pt spacer.

Figure10 shows the oscillatory variation of the mangetization reversal behaviors of the [Pt(2.0 nm)/Co(0.3 nm)]$_6$/Pt(t_{Pt})/Co(8.5 nm)/FeMn(25.0 nm) multilayers and the Co(8.5 nm)/Pt(t_{Pt})/{Co(0.3 nm)/[Pt(2.0 nm)/Co(0.3 nm)]$_5$}/FeMn(25.0 nm) multilayers as the t_{Pt} varying. The Co(8.5 nm) layer has in-plane anisotropy. The $(Pt/Co)_6$ or $[Co/(Pt/Co)_5]$ periods, regarded as a combined FM layer, has perpendicualr anisotropy. The interlayer exchange coupling between the Co(8.5 nm) layer and the $(Pt/Co)_6$ periods oscillates with the inrement of the Pt spacer thickness (t_{Pt}). It can be seen in Fig.10(a) that the the H_{ex} and the hysteresis (*Hys.-area*) for the $[Co/(Pt/Co)_5]$ periods in the Co/Pt(t_{Pt})/$[Co/(Pt/Co)_5]$/FeMn multilayers are oscillatory. The period of the oscillation is about 3.2 nm, which is close to that of the interlayer coupling between two Co layers in the $(Pt/Co)_n$ system [36].

The $(Pt/Co)_6/Pt(t_{Pt})/Co/FeMn$ multilayers, as seen in Fig.10(b), exhibit zero H_{ex} and little changes of hysteresis area. However, some of their loops show vertical shift accompanied with the asymmetric anomaly. The vertical shift of the loops is shown in the inset of Fig.10(b) as a shift of the remanent magnetization (M_r-*shift*) or a shift of the hysteresis zone (*Hys.-shift*). As t_{Pt} varies, the *M*-fluctuation on the left side (H<0) has little changes. Meanwhle, the M_r-*shift*, the *Hys.-shift*, and the fluctuation of *M* on the right side (H>0), oscillate synchronously. When t_{Pt}=6.6 nm, the right-side *M*-peak is just like that in the Co/FeMn bilayer. When t_{Pt}=4.6 nm, the right-side *M*-peak

is suppressed by the interlayer coupling. It means that the interlayer coupling between the $(Pt/Co)_6$ peroids and the Co(8.5 nm) single layer has an significant influence on the magnetic structure within the Co single layer.

The in-plane loops were also measured by VSM (in PPMS). The MD rotates within the film plane with the angular step of 10°. The loops both for t_{Pt}=4.6 nm and for t_{Pt}=6.6 nm show in-plane EBs. The EB for these loops with two different t_{Pt} have something in common. When the MD is along the PD, H_{ex} and H_c reach their maximum. When the MD is perpendicular to the PD, H_{ex} is zero and H_c reaches its minimum. However, their H_{ex} and H_c vary in different manner. The maximum of the EB for t_{Pt}=6.6 nm is higher than that for t_{Pt}=4.6 nm. There is a Plateau in the H_c-t_{Pt} curve for t_{Pt}=6.6 nm as well as in the H_{ex}-t_{Pt} curve for t_{Pt}=4.6 nm.

It can be known from Fig.10 and Fig.11 that the interlayer exchange coupling between the Co(8.5 nm) layer and the $(Pt/Co)_6$ periods is ferromagnetic and antiferromagnetic when t_{Pt}=6.6 nm and t_{Pt}=4.6 nm, respectively. The discrepancy of the angular dependences of the EB and the coercivity in the in-plane loops and the variation trend of *M*-fluctuation in the perpendicular loops between t_{Pt}=6.6 nm and t_{Pt}=4.6 nm is associated with influence of the interlayer coupling on the spatial pathway of moment rotation during the magnetization reversal. It is not a surprise that interlayer coupling at the side away from the FM/AFM interface could affect the EB in that the magnetic structure inside the FM layer is also a determinant of the EB, especially for a thick FM layer having inhomogeneous magnetic structure in different depth.

Taking account to the demagnetization, the perpendicular exchange length of the Co layer is about 2.9 nm. When Co layer are pinned by the FeMn layer, the rotation of the magnetic moments of Co at the FM/AFM interface is harder than that of the moments located away from the interface. That makes the inconsistency of the orientation of the Co moments during the magnetization reversal. When t_{Co}=8.0 nm, the Co layer is thick enough to form a planar exchange spring or even an incomplete planar domain wall. Since the FM layer rotate incoherently during the reversal, the S-W model based on the coherent rotation does not work well here. A more senior model should be employed to interpret the unique AMRBs we observed.

A third condition for the unique AMRB we observed is the AFC at the FM/AFM interface. There are some clues about the dominating AFC, which have been shown in Fig.4(B) and Fig.5(c and e). One result of the AFC is the multiple metastable state of the spin configuration during the reversal process. The fluctuation of *M* can be attributed to the hopping among the multiple metastable states. Here we give a probable schematic illustration of the strange asymmetric *M*-peaks in the loops in framework of the cooperation of the two AMRB origins and the AFC.

The hysteresis loop (C) in Fig.4 (t_{Co}=8.0 nm) could be divided into five stages (marked with I~V in the figure) according to the signal of d*M*/d*H*. The signal of d*M*/d*H* is positive in stage I, III, and V, whereas is negative in stage II and IV. The *M*-peaks denote the irreversible mutation of the spin structure during the magnetization reversal, which is often observed in the $M_\perp$-*H* curves ($M_\perp$ represents the projection component of *M* perpendicular to the field direction) [6,37]. Usually

there are only two irreversible stages in a whole *M*-*H* loop (one in each reversal branch). However, due to the AFC, four irreversible nucleation-propagation stages appear in a single loop here. The negative d*M*/d*H* in stage II and IV seem as if breaking the second law of thermodynamics. Actually, it means that during the magnetization reversal, the restoring and relieving of the exchange coupling energy both at the FM/AFM interface and within the FM layer should be considered. In our Co/FeMn bilayers, as the Co layer is rather thick and the PD is non-collinear with the anisotropy, a planar exchange spring could be formed in the Co layer. The total energy could be written as:

$$E_{\text{total}} = E_{\text{Z}} + E_{\text{FS}} + E_{\text{INT}} \quad (1)$$

Where E_{Z} is the Zeeman energy of the bilayer, E_{FS} is the exchange energy of the exchange spring in the FM layer, and E_{INT} is the interfacial coupling energy, including the coupling between the FM spins and the rotatable UCAS, and the coupling between the rotatable and the pinned AFM spins. Consequently, the magnetization could vary against the external field at the cost of the E_{FS} or E_{INT}. There are multiple metastable spin configurations during the magnetization reversal in the competition of E_{Z}, E_{INT}, and E_{FS}. The most favorable orientations of the FM spins, as well as that of the pinned and rotatable UCAS, depend jointly on the pinning strength derived from the AFM layer, the external field, and the depth of the spins.

Figure12(a) gives a schematic illustration of the spin structure of the perpendicular induced Co/FeMn bilayer, in which the orientations of the spins at the top and bottom interfaces of the FM layer ($\boldsymbol{s}_{\text{FTI}}$ and $\boldsymbol{s}_{\text{FBI}}$) are discrepant. Similar to the case in the FM/spin-glass systems [33], we consume that the interfacial uncompensated AFM net spins ($\boldsymbol{s}_{\text{UCN}}$) is antiferromagnetic-coupled to the $\boldsymbol{s}_{\text{FTI}}$ and pinned by the compensated AFM spins ($\boldsymbol{s}_{\text{AFP}}$). The orientation of the $\boldsymbol{s}_{\text{UCN}}$ is jointly determined by the anisotropy and the interfacial exchange coupling. Here we assume that K_{E} and K_{U} of $\boldsymbol{s}_{\text{UCN}}$ are both tilted by the same angle.

The reversal process of the spins in different depth is shown in Fig.12(b). In stage II and IV, the $\boldsymbol{s}_{\text{UCN}}$ and the FM spins flip into the nearly opposite directions, accompanied with the energy exchange between E_{Z} and (E_{FS}+E_{INT}). It can be seen from Fig.12(b) that the reversal process is neither symmetric nor reversible, which is a typical character of type-II AMRBs. In the case of type-II AMRB, the FM spins rotate along the semicircle in accordance with the side of PD when the pining effect is strong enough [5,6]. However, in our Co/FeMn bilayers, taking into account the antiferromagnetic interfacial coupling, the $\boldsymbol{s}_{\text{UCN}}$ rotate along the side of PD while the FM spins rotate along the semicircle against the side of PD. Irreversible flipping of $\boldsymbol{s}_{\text{UCN}}$ and $\boldsymbol{s}_{\text{FTI}}$ takes place synchronously in stage II and IV respectively.

In addition, the stage II and the stage IV are different. Since the FM/AFM interfacial coupling is antiferromagnetic, E_{FS} and E_{INT} are in competition. In stage II, the E_{INT} increase, whereas the E_{FS} decrease. The driving force of the evolution in this stage is the reduction of E_{FS}. The opposite is the case in stage IV.

Moreover, it is obviously not a simple type-II AMRB, but a AMRB with dual origin here. The

incoherency of the FM layer, as the basis of type-I AMRB, is also indispensable to this novel AMRB, too. The inhomogeneous FM layer yields the E_{FS}, which is crucial to the sudden inversion of the spins in stage II. Therefore, the unusual *M*-peak at the right side of the loops (stage II~III) is strongly revelent to the incoherent reversal within the FM layer.

It seems curious that the AGM and the VSM (in PPMS) measurments show different results in the loop shape. In fact, it could be attributed to the influence of the small alternating gradient component of the AGM measuring field on the reversal of the interfacial spins.

Since the AFC was observed in our perpendicular induced Co/FeMn bilayers, there should be three minimum energy states in the middle of the reversal course (stage III as shown in Fig.3). In most cases (e.g. in the PPMS measurement, as shown in Fig.12(c) by the dot curves), the metastable configuration of the interfacial spins is inaccessible in that energetic reduction in forming the metastable phase is small and the energetic barrier for the phase transition is high.

However, the AGM measurement is of special measuring principle. The AGM measurement field consists of a DC sweeping component (up to 15 kOe) and a small alternating gradient component (5~20 Oe/cm, 350~400 Hz). As it is also in a gradient form, the perpendicular demagnetization (shape anisotropy) is affected cumulatively by the alternating gradient field. Then the domain nucleation of more stable phases during the magnetization reversal is affected. Although the amplitude of the gradient field is rather small, the activating energy derived from the alternating gradient field is much than the thermal activation at room temperature. The alternating gradient field could provide adequate activating energy to help the nucleation of the metastable phase. The interfacial spins would not flip over without the aid of the alternating gradient field. That might be the reason why the odd *M*-fluctuations are not observed in the VSM (PPMS) measurements.

In summary, the AMRBs in the Co/FeMn bilayers grown under the perpendicular magnetic field (hard axis of the FM layer) were investigated. The bilayer has an oblique PD and contains a quite thick Co layer, which means the conditions for two intrinsic AMRB origins (i.e. competing anisotropy and inhomogeneous magnetic structures) are fulfilled. Novel AMRBs, including a positive EB and the odd shape of the *M*-*H* loops, are observed in the perpendicular magnetization reversal courses by means of AGM measurement. The novel AMRBs were not found in the in-plane loops. The dependence of these AMRBs on t_{Co} as well as t_{FeMn} is investigated. Unexpectedly, the critical AFM layer thickness for these AMRBs is larger than that for the loop shift. Besides, there is also a critical range of the FM layer thickness. The critical FM thickness is relevant to the competition of the anisotropy, while the critical AFM thickness is relevant to the competition of the exchange coupling. The coexistence of the two critical thicknesses indicates that both origins are essential to the development of these novel AMRBs. The reversal courses were illustrated by a model based on tilted PD, incoherent spin rotation, and antiferromagnetic FM/AFM interfacial coupling. The present work found a connection between the two intrinsic AMRB origins discovered before. The compatibility of the two AMRB origins was confirmed.

They can coexist and cooperate in particular EB systems. The unity of the two AMRB origins was also discussed. They could be combined as the spatial symmetry breaking in the competition between the energetic terms, such as the anisotropy energy, the Zeeman energy, and the exchange coupling energy throughout the EB multilayers.

The authors would like to thank Li Sun for helpful discussions and advices. This work is supported by the National Science Foundation of China (Grant Nos. 50831002, 50871014, 50971021, and 51071023) and NSF (Grant No. DMR-0821284), and NASA IDEAS-ER (Grant Nos. NNX10AM80H and NNX07AO30A).

* Email: ghyu@mater.ustb.edu.cn

[1] V. I. Nikitenko, V. S. Gornakov, A. J. Shapiro, R. D. Shull, Kai Liu, S. M. Zhou, and C. L. Chien, Phys. Rev. Lett. **84**, 765 (2000).

[2] Z. Y. Liu, and S. Adenwalla, Phys. Rev. B **67**, 184423 (2003).

[3] A. Hoffmann, Phys. Rev. Lett. **93**, 097203 (2004).

[4] Zhi-Pan Li, O. Petracic, R. Morales, J. Olamit, X. Batlle, Kai Liu, and Ivan K. Schuller, Phys. Rev. Lett. **96**, 217205 (2006).

[5] B. Beckmann, U. Nowak, and K. D. Usadel, Phys. Rev. Lett. **91**, 187201 (2003).

[6] J. Camarero, J. Sort, A. Hoffmann, J. M. García-Martín, B. Dieny, R. Miranda, and J. Nogués, Phys. Rev. Lett. **95**, 057204 (2005).

[7] L. Sun, P. C. Searson, and C. L. Chien, Phys. Rev. B **71**, 012417 (2005).

[8] D. Spenato, V. Castel, S. P. Pogossian, D. T. Dekadjevi, and J. Ben Youssef, Appl. Phys. Lett. **91**, 062515 (2007).

[9] J. Camarero, J. Miguel, J. B. Goedkoop, J. Vogel, F. Romanens, S. Pizzini, F. Garcia, J. Sort, B. Dieny, and N. B. Brookes, Appl. Phys. Lett. **89**, 232507 (2006).

[10] F. Romanens, S. Pizzini, J. Sort, F. Garcia, J. Camarero, F. Yokaichiya, Y. Pennec, J. Vogel, and B. Dieny, Eur. Phys. J. B **45**, 185 (2005).

[11] J. McCord, R. Schäfer, R. Mattheis, and K.-U. Barholz, J. Appl. Phys. **93**, 5491 (2003).

[12] V. I. Nikitenko, V. S. Gornakov, L. M. Dedukh, Yu. P. Kabanov, A. F. Khapikov, A. J. Shapiro, R. D. Shull, A. Chaiken, and R. P. Michel, Phys. Rev. B **57**, R8111 (1998).

[13] M. Czapkiewicz, T. Stobiecki, and S. van Dijken, Phys. Rev. B **77**, 024416 (2008).

[14] F. Romanens, S. Pizzini, F. Yokaichiya, M. Bonfim, Y. Pennec, J. Camarero, J. Vogel, J. Sort, F. Garcia, B. Rodmaq, and B. Dieny, Phys. Rev. B **72**, 134410 (2005).

[15] G. Malinowski, S. van Dijken, M. Czapkiewicz, and T. Stobiecki, Appl. Phys. Lett. 90, 082501 (2007).

[16] C. Leighton, M. R. Fitzsimmons, P. Yashar, A. Hoffmann, J. Nogués, J. Dura, C. F. Majkrzak, and Ivan K. Schuller, Phys. Rev. Lett. **86**, 4394 (2001).

[17] J. Moritz, D. S. Van, and J. M. Coey, Eur. Phys. J. B **45**, 1913(2005).

[18] R. Morales, Zhi-Pan Li, O. Petracic, X. Batlle, Ivan K. Schuller, Justin Olamit, and Kai Liu,

Appl. Phys. Lett. **89**, 072504 (2006).

[19] X. P. Qiu, D. Z. Yang, S. M. Zhou, R. Chantrell, K. O'Grady, U. Nowak, J. Du, X. J. Bai, and L. Sun, Phys. Rev. Lett. **101**, 147207 (2008).

[20] X. P. Qiu, Z. Shi, S. M. Zhou, J. Du, X. J. Bai, R. Chantrell, and L. Sun, J. Appl. Phys. **106**, 063903 (2009).

[21] M. K. Chan, J. S. Parker, P. A. Crowell, and C. Leighton, Phys. Rev. B **77**, 014420 (2008).

[22] S. Brems, D. Buntinx, K. Temst, C. Van Haesendonck, F. Radu, and H. Zabel, Phys. Rev. Lett. **95**, 157202 (2005).

[23] E. Girgis, R. D. Portugal, H. Loosvelt, M. J. Van Bael, I. Gordon, M. Malfait, K. Temst, C. Van Haesendonck, L. H. A. Leunissen, and R. Jonckheere, Phys. Rev. Lett. **91**, 187202 (2003).

[24] J. Eisenmenger, Zhi-Pan Li, W. A. A. Macedo, and Ivan K. Schuller, Phys. Rev. Lett. **94**, 057203 (2005).

[25] M. R. Fitzsimmons and P. Yashar, C. Leighton, Ivan K. Schuller, J. Nogués, C. F. Majkrzak, and J. A. Dura, Phys. Rev. Lett. **84**, 3986 (2000).

[26] W.-T. Lee, S. G. E. te Velthuis, G. P. Felcher, F. Klose, T. Gredig, and E. D. Dahlberg, Phys. Rev. B **65**, 224417 (2002).

[27] D. M. Engebretson, W. A. A. Macedo, Ivan K. Schuller, P. A Crowell, and C. Leighton, Phys. Rev. B **71**, 184412 (2005).

[28] A. Paul, M. Buchmeier, C. M. Schneider, and T. Brückel, J. Appl. Phys. **101**, 123913 (2007).

[29] J. Nogués, D. Lederman, T. J. Moran, and Ivan K. Schuller, Phys. Rev. Lett. **76**, 4624 (1996).

[30] T. Gredig, I. N. Krivorotov, P. Eames, and E. D. Dahlberg, Appl. Phys. Lett., **81**, 1270 (2002).

[31] F. Canet, S. Mangin, C. Bellouard and M. Piecuch, Euro. Phys. Lett., **52**, 594 (2000).

[32] Y. Henry, S. Mangin, T. Hauet, and F. Montaigne, Phys. Rev. B, **73**, 134420 (2006).

[33] M. Ali, P. Adie, C. H. Marrows, D. Greig, B. J. Hickey , and R. L. Stamps, Nat. Mater. **6**, 70 (2007).

[34] S. K. Mishra, F. Radu, H. A. Dürr, and W. Eberhardt, Phys. Rev. Lett., **102**, 177208 (2009).

[35] F. Radu and H. Zabel, Springer Tracts in Modern Physics **227**, 97-184, (2008).

[36] J. W. Knepper, and F. Y. Yang, Phys. Rev. B **71**, 224403 (2005).

[37] C. Hamann, J. McCord, L. Schultz, B. P. Toperverg, K. Theis-Bröhl, M. Wolff, R. Kaltofen, and I. Mönch, Phys. Rev. B **81**, 024420 (2010).

FIGURE CAPTIONS:

FIG.1 *M-H* curves of the Co(t_{Co})/FeMn(13.0 nm) bialyers along two in-plane directions perpendicular to each other (X and Y). (Measured by VSM in PPMS. Normalized by V_{Co}.)

FIG.2 *M-H* curves of the Co(t_{Co})/FeMn(13.0 nm) bialyers along the direction perpendicular to the film plane. (Measured by VSM in PPMS. Normalized by the saturation magnetization.)

FIG.3 Dependence of the saturation magnetization on the Co layer thickness in Co(t_{Co})/FeMn(13.0 nm) bialyers. (Z): the direction perpendicular to the film plane; (X and Y): two in-plane directions perpendicular to each other. (Measured by VSM in PPMS. Normalized by the volume of Co (V_{Co}).) Inset: dependence of the saturation magnetization on the Co layer thickness in Co(t_{Co})/FeMn(25.0 nm) bialyers. (measured by AGM. Normalized by the nominal saturation magnetization for t_{Co}=0.)

FIG.4 Perpendicular *M-H* curves of the Co(t_{Co})/FeMn(25.0 nm) bialyers in 3×3 mm^2 pieces. Black: from $+H_s$ to $-H_s$, Red: from $-H_s$ to $+H_s$. According to the signal of the dM/dH, the magnetization reversal course in loop (C) is divided into five stages, marked as (I)~(V). The center of loop (D) is enlarged to the inset for clarity.

FIG.5 Perpendicular *M-H* curves of the Co(8.0 nm)/FeMn(t_{FeMn}) bialyers (in 3×3 mm^2 pieces) measured by AGM. Black: from $+H_s$ to $-H_s$, Red: from $-H_s$ to $+H_s$. The maximum of the measuring field is 15 kOe. Only the central parts of the loops are shown here for clarity.

FIG.6 *M-H* loops of the Co(t_{Co})/FeMn(13.0 nm) bialyers along a random in-plane direction. (X,Y) represents a random direction within the film plane. (Measured by AGM. Normalized by V_{Co}.)

FIG.7 *M-H* loops of the Co(8.0 nm)/FeMn(t_{FeMn}) bialyers along a random in-plane direction (X,Y). (Measured by AGM. Normalized by V_{Co}.)

FIG.8 *M-H* loops of the Co(t_{Co})/FeMn(13.0 nm) bialyers along a random in-plane direction (X,Y). (Measured by VSM in PPMS. Normalized by V_{Co}.)

FIG.9 *M-H* loops of the Co(8.0 nm)/FeMn(t_{FeMn}) bialyers along two in-plane directions perpendicular to each other (X and Y). (Measured by VSM in PPMS. Normalized by V_{Co}.)

FIG.10 (a): *M-H* loops of Co(8.5 nm)/Pt(t_{Pt})/[Co/(Pt/Co)$_5$]/FeMn multilayers, Inset: dependence of the H_{ex} (solid circle) and the *Hys.-area* (empty circle) on the t_{Pt}. (b): *M-H* loops of [Pt/Co]$_6$/Pt(t_{Pt})/Co(8.5 nm)/FeMn multilayers, Inset: dependence of the M_r-*shift* (solid circle) and the *Hys.-shift* (empty circle)

on t_{Pt}. *Hys.-area* and *Hys.-shift* are the entire loop sum of energy: *Hys.-area* = $-\Sigma M\delta H$, *Hys.-shift* = $-\Sigma|M|\delta H$. .

Fig.11 Dependence of the exchange bias field (H_{ex}) and coercivity (H_C) on the measuring direction for the Co(8.5 nm)/Pt(t_{Pt})/[Co/(Pt/Co)$_5$]/FeMn (t_{Pt}=4.6 and 6.6 nm) multilayers. (Measured by VSM in PPMS.)

Fig.12 (a): Schematic illustration of the spin structure of the perpendicular induced Co/FeMn bilayer (6.4 nm<t_{Co}<10.0 nm, t_{FeMn}>12.0 nm). Z: the direction perpendicular to the film plane; X,Y: an random direction in the film plane. (b and c): The five-stage scheme of the reversal course. The thick arrows in (a and b) represent the orientations of the spins located at four different depths respectively. Empty blue arrow: $\boldsymbol{s}_{FTI}$; black solid arrow: $\boldsymbol{s}_{FBI}$; red solid short arrow: $\boldsymbol{s}_{UCN}$; red empty short arrow: $\boldsymbol{s}_{AFP}$. The arrow arcs outside the gray circle represent the rotating courses of the spins. The green dot lines or dot arrows represent the pinning direction. (c): the dependence of the orientations of $\boldsymbol{s}_{FTI}$, $\boldsymbol{s}_{FBI}$, and $\boldsymbol{s}_{UCN}$, on the measuring field during the reversal course. Solid curves: in AGM measurement; dot curves: in VSM (PPMS) measurement.

FIGURE 1 – Y. Liu et al.

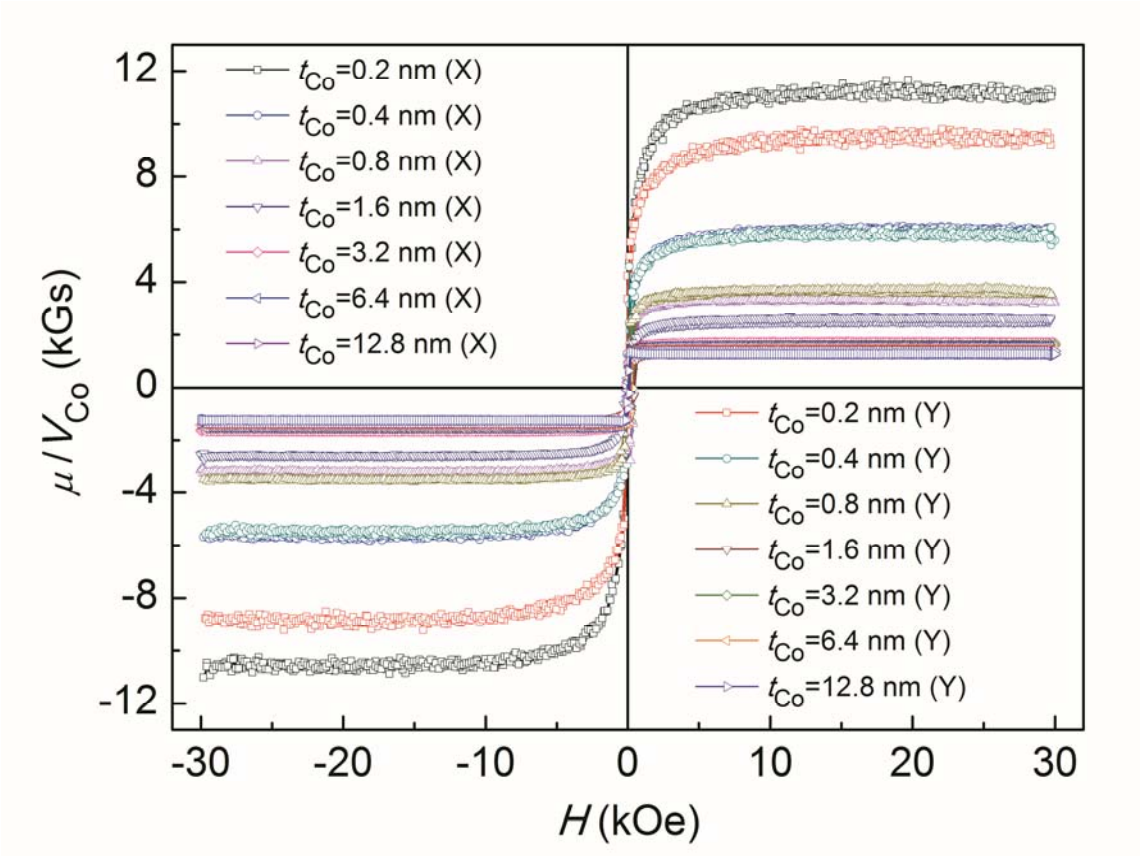

FIGURE 2 – Y. Liu et al.

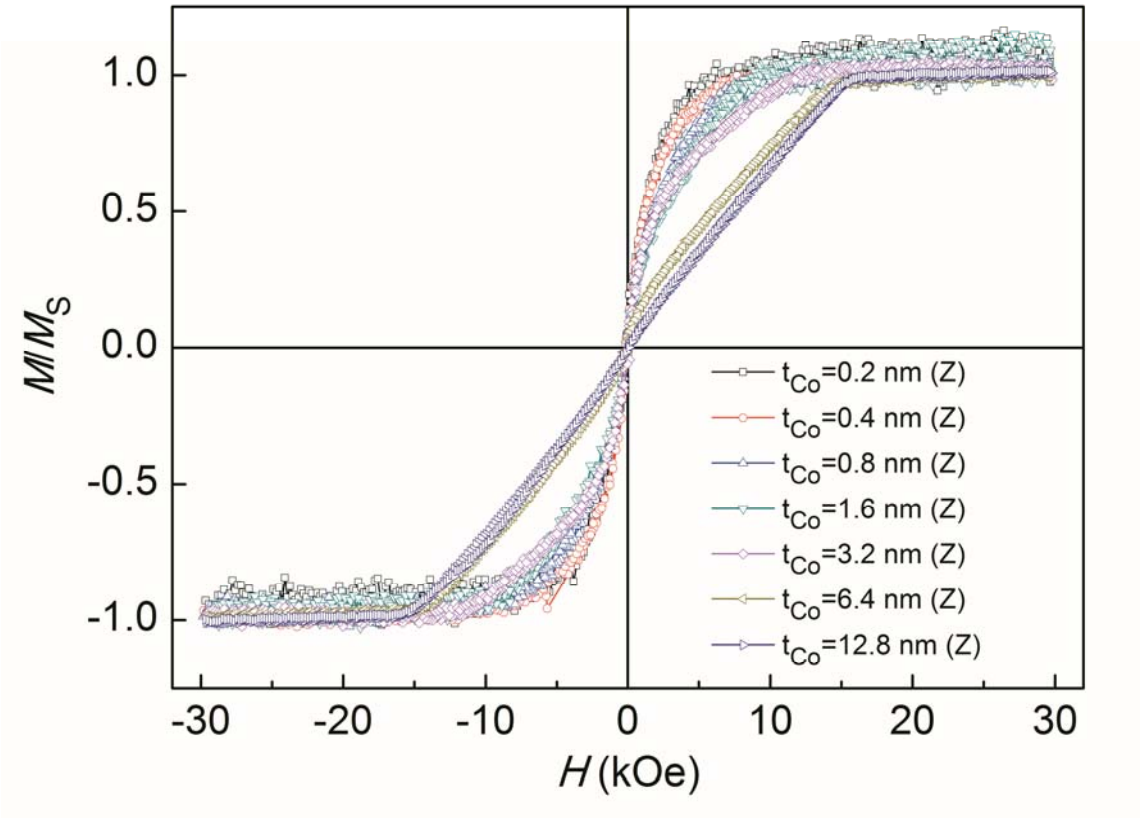

FIGURE 3 – Y. Liu et al.

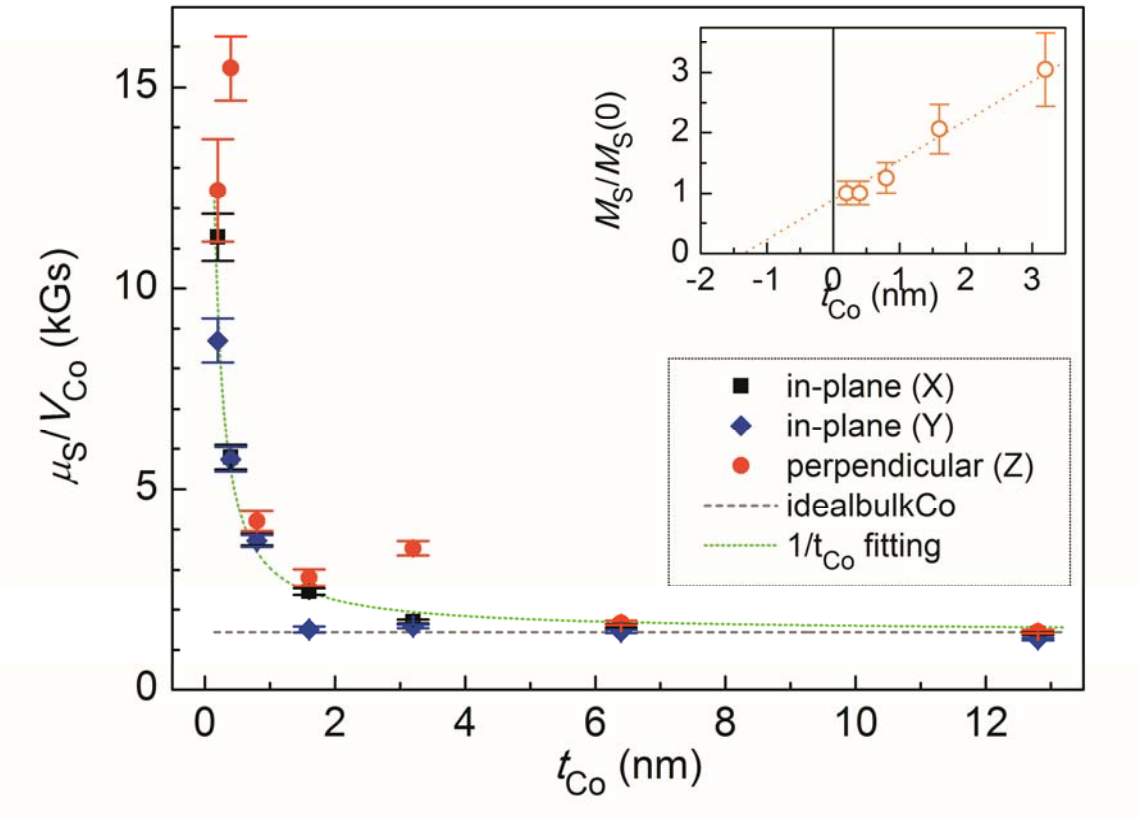

FIGURE 4 – Y. Liu et al.

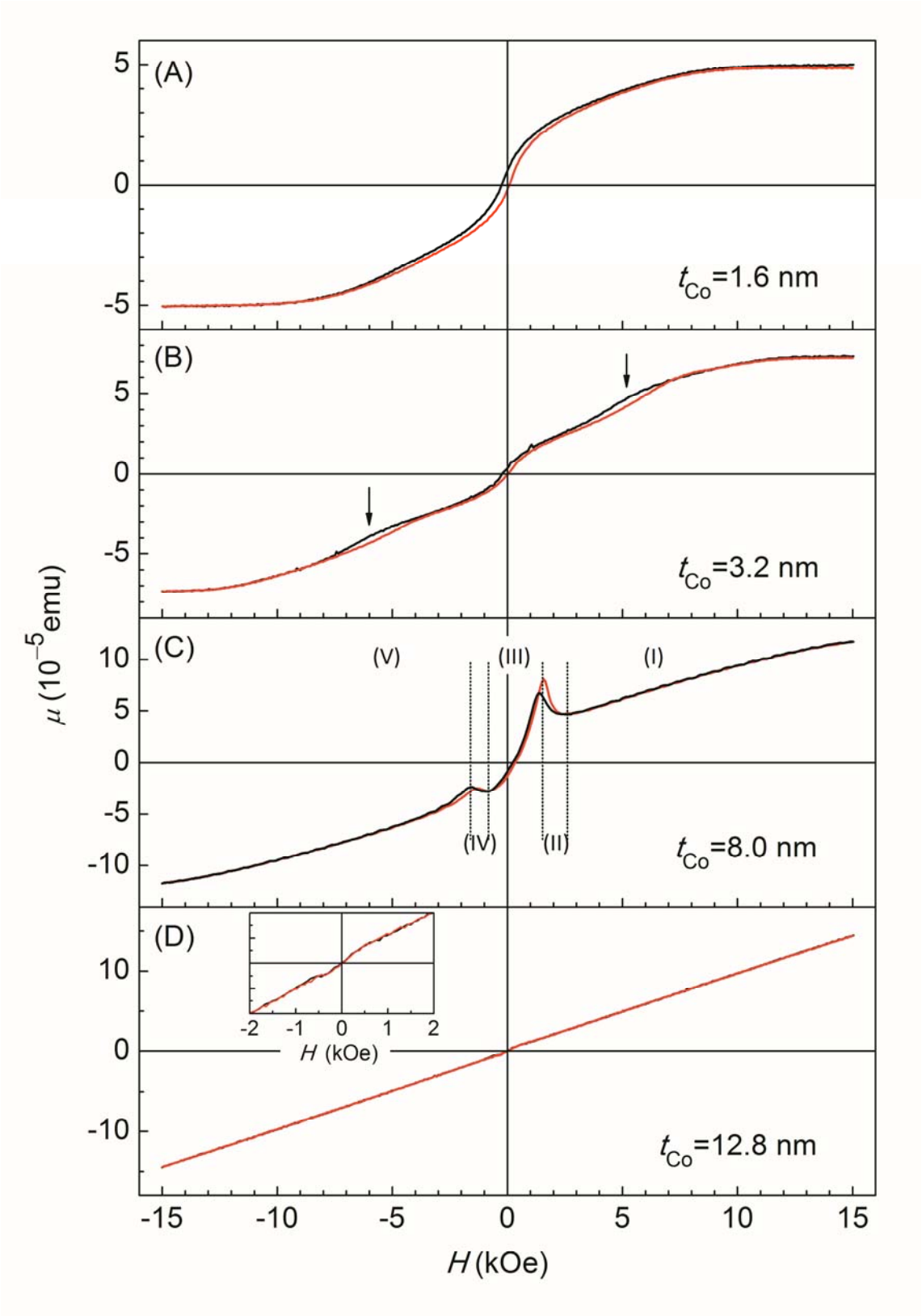

FIGURE 5 – Y. Liu et al.

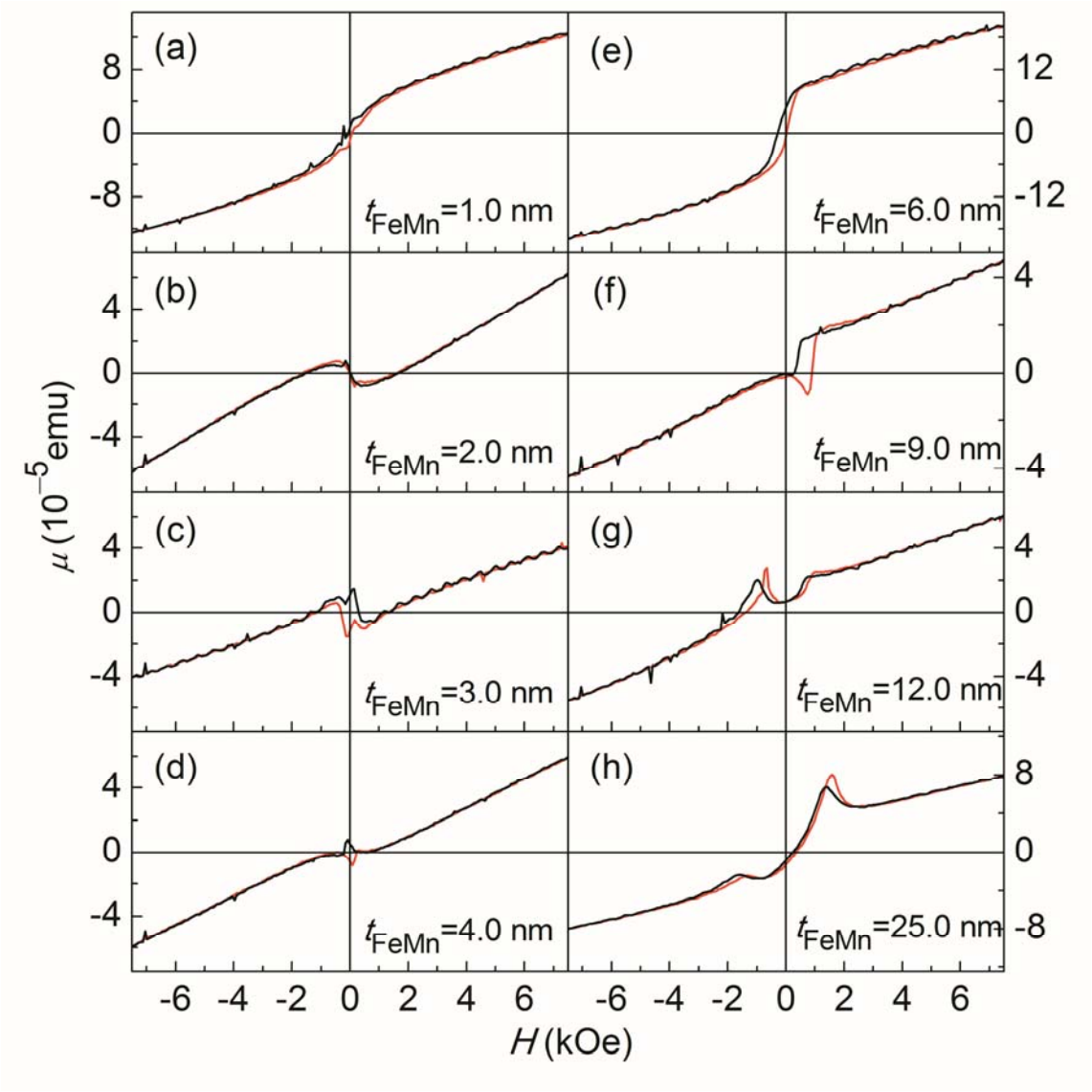

FIGURE 6 – Y. Liu et al.

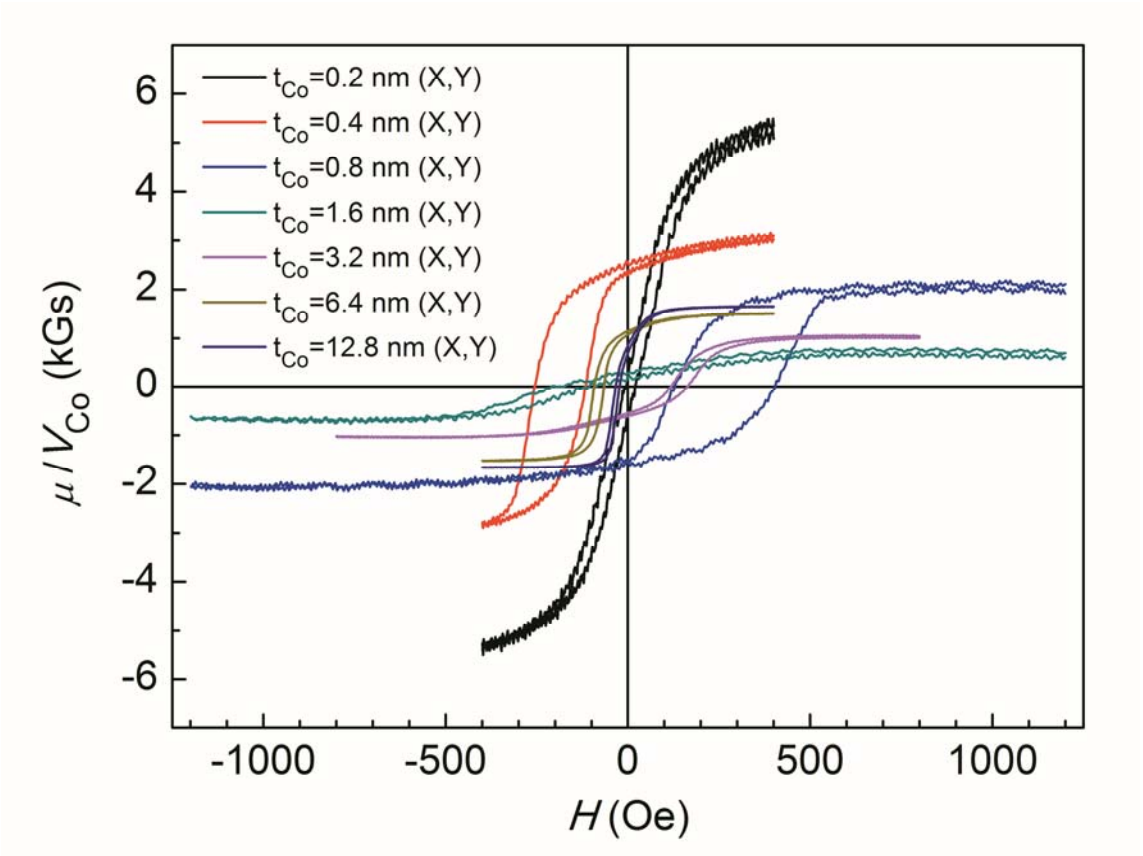

FIGURE 7 – Y. Liu et al.

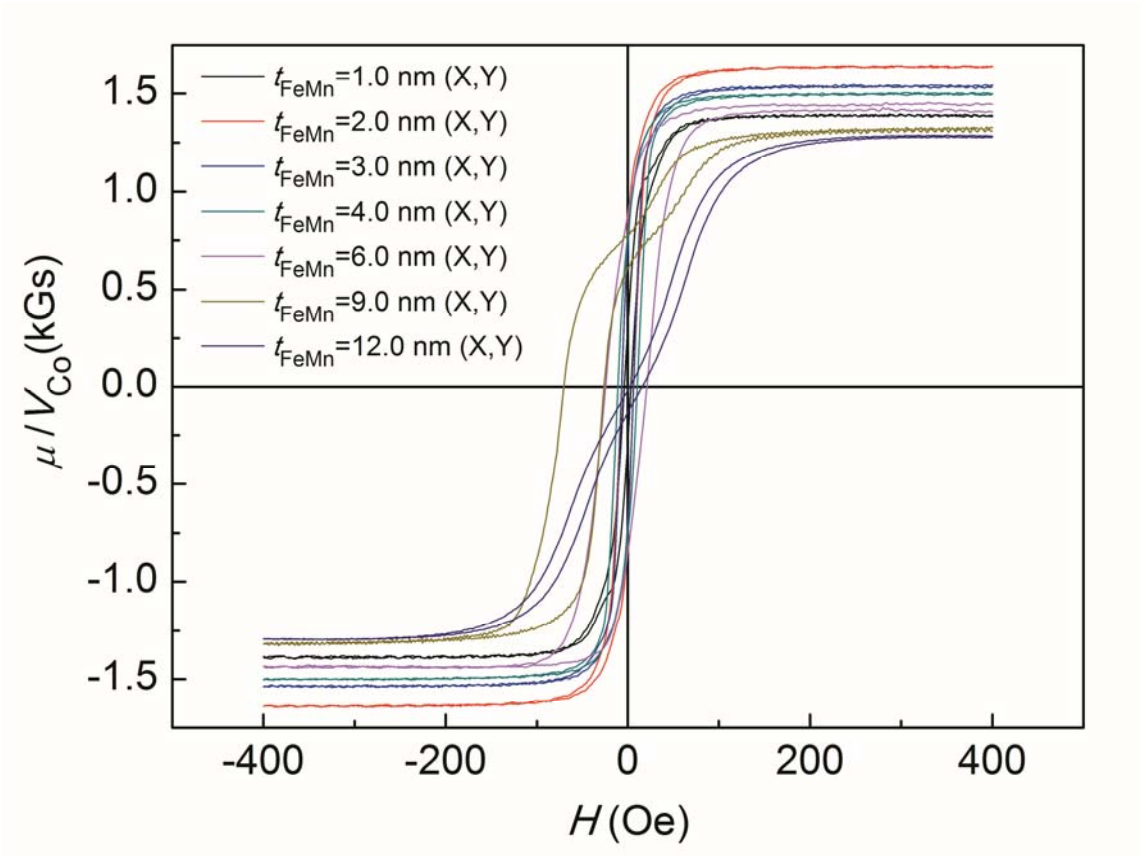

FIGURE 8 – Y. Liu et al.

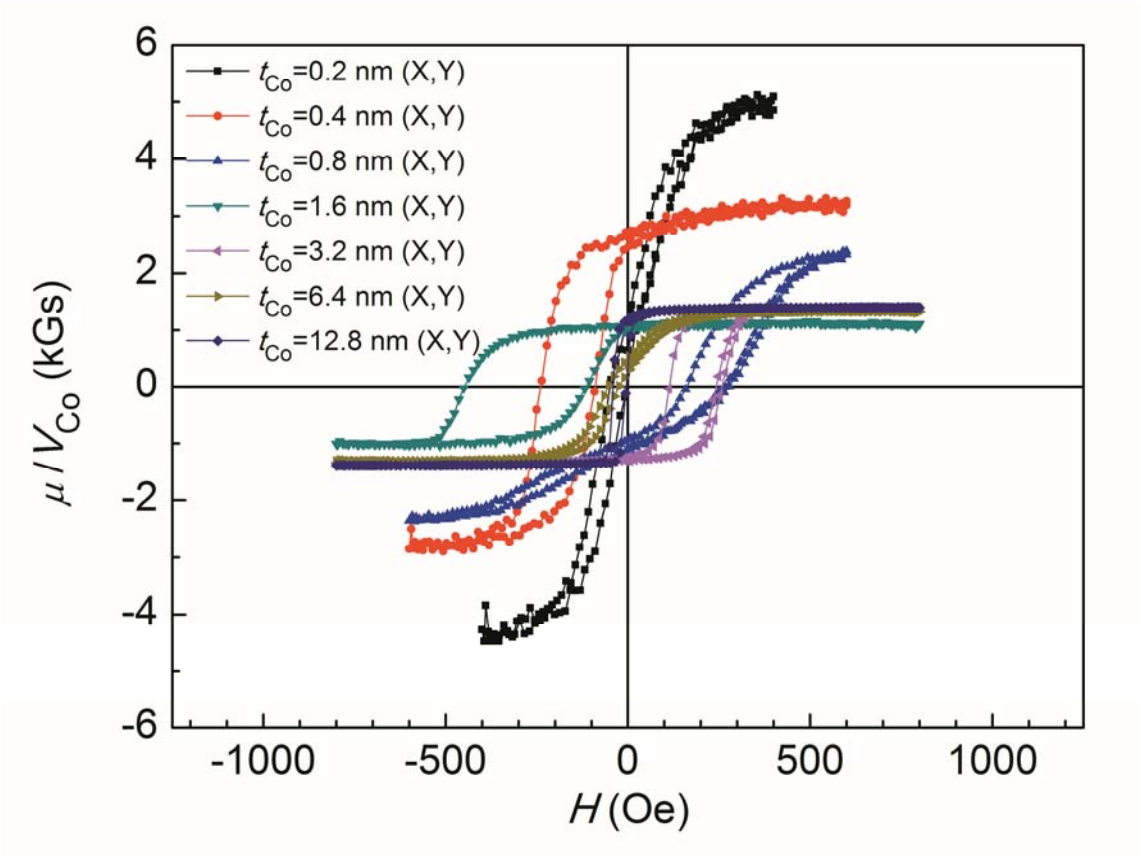

FIGURE 9 – Y. Liu et al.

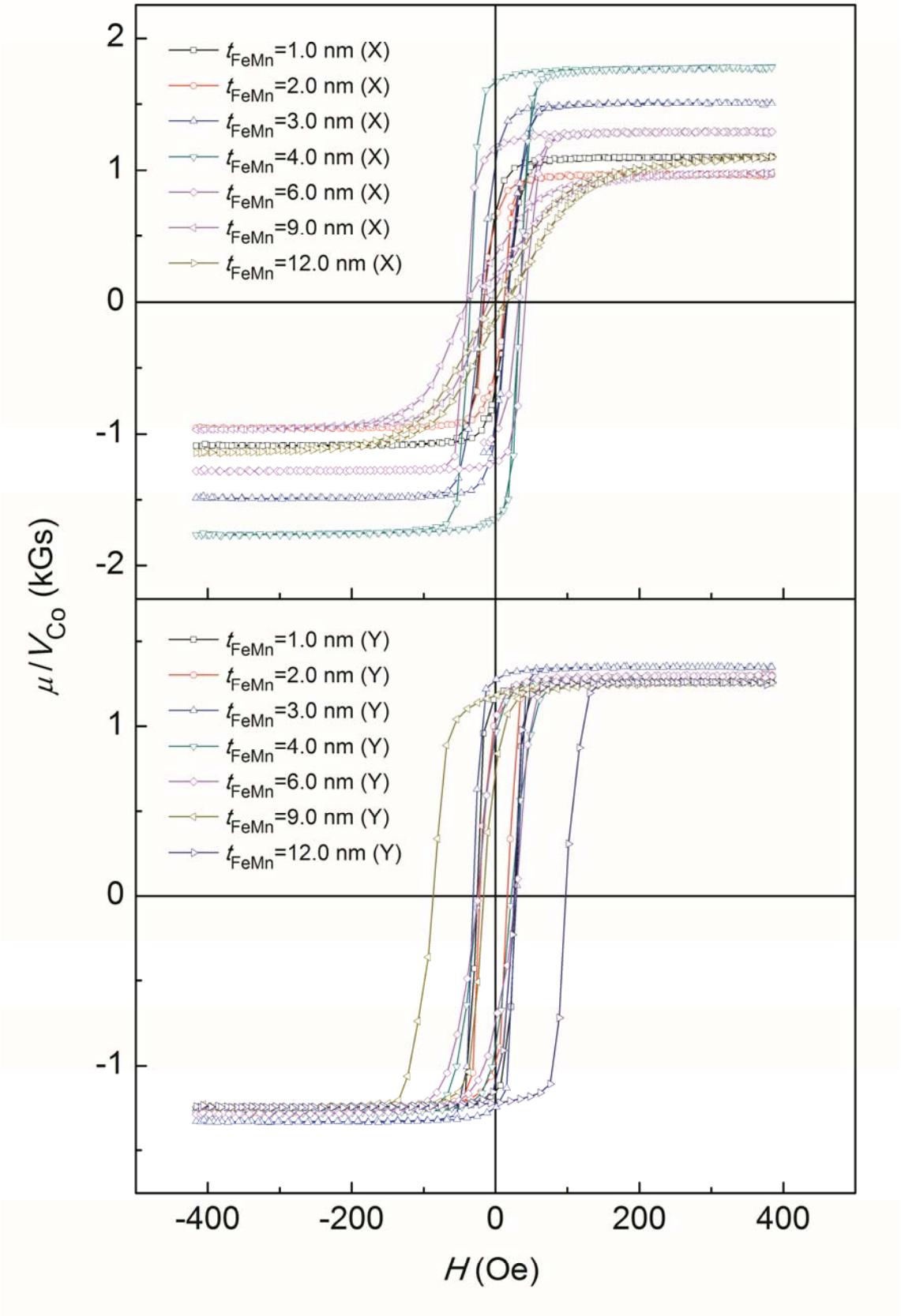

FIGURE 10 – Y. Liu et al.

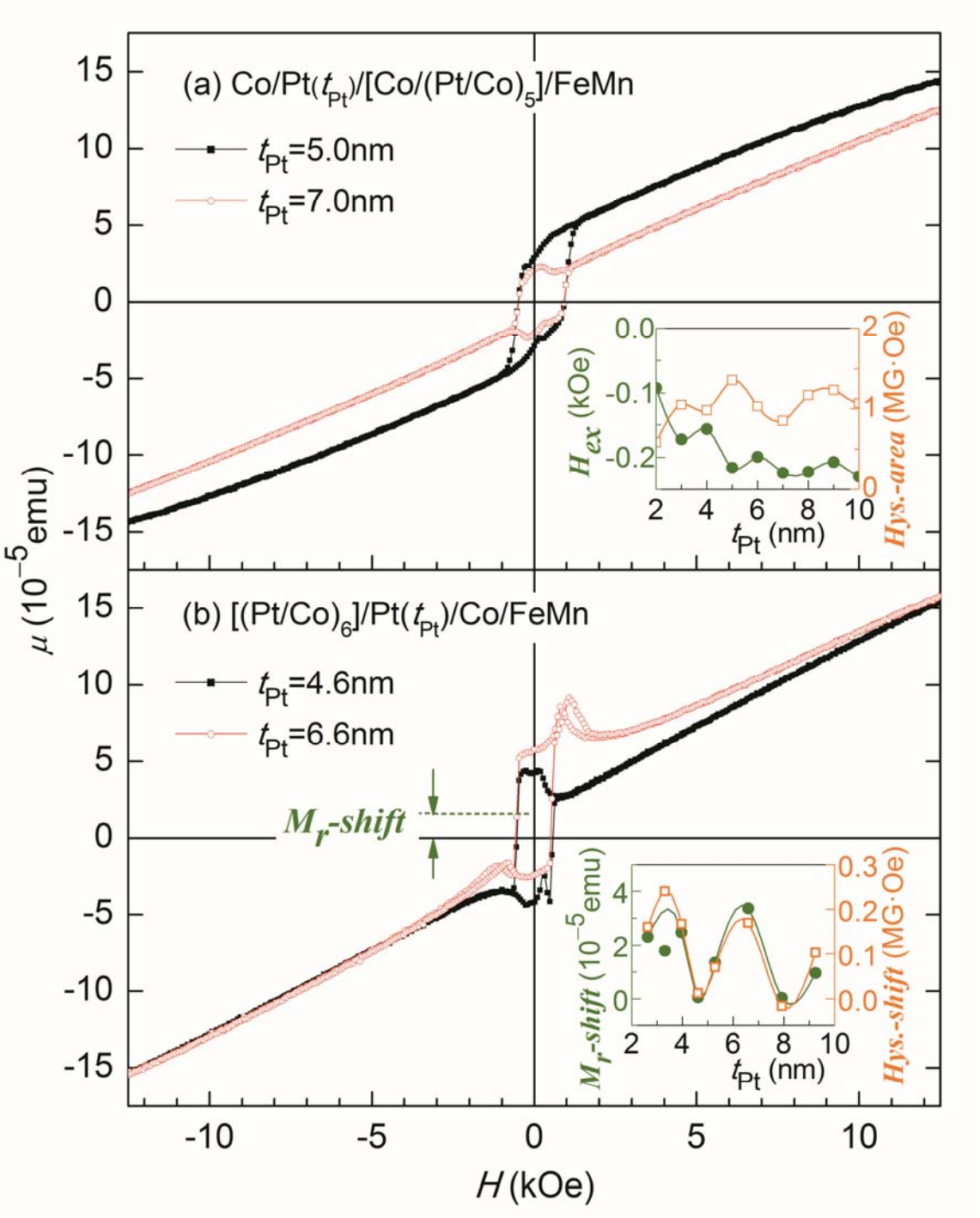

FIGURE 11 – Y. Liu et al.

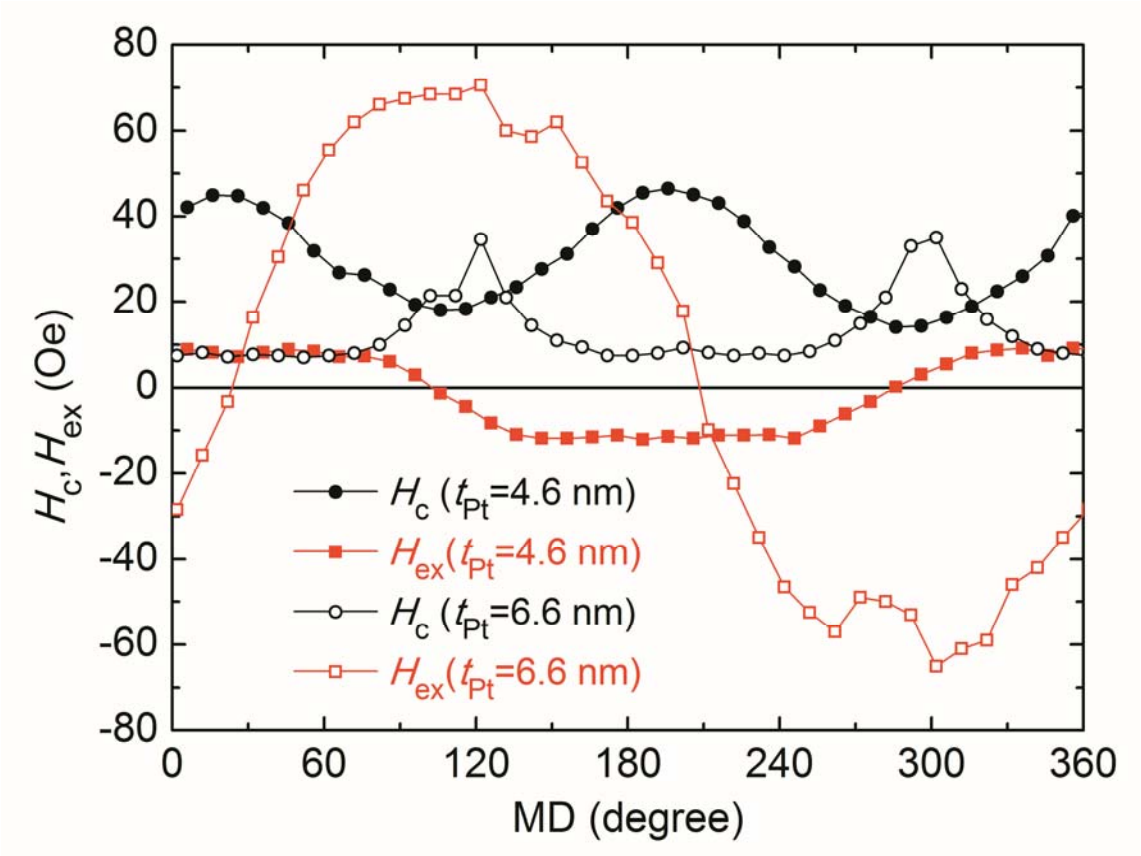

FIGURE 12 – Y. Liu et al.